

Implications on oil trapping in the Kifl field of Iraq through geophysical investigations

Mohanad AL-Farhan ^{a, b}, Behrooz Oskooi ^{a, *}, Maysam Abedi ^c, Vahid E. Ardestani ^a, Amar AL-Khalidy ^d

^a *Institute of Geophysics, University of Tehran, Tehran, Iran.*

^b *Directorate of Education of Basra, Ministry of Education, Basra, Iraq.*

^c *School of Mining Engineering, College of Engineering, University of Tehran, Tehran, Iran.*

^d *Department of Applied Geology, College of Sciences, University Babylon, Babylon Iraq.*

Article History:

Received: 28 April 2022.

Revised: 06 June 2022.

Accepted: 13 June 2022.

ABSTRACT

Potential field geophysical measurements were conducted in the west of Kifl region in central Iraq to image a plausible oil-trapping reservoir. Ground-based magnetometry and gravimetry surveys were conducted to investigate this region by covering an area of 16×24 km by designing a regular grid spacing of 250 m. After preprocessing potential field data, different filters were utilized to separate the residuals from the regional anomalies. The complicated tectonic setting of the studied area was imaged by recognition of the fault system through simulation of the magnetic and gravity anomalies, which facilitates the configuration display of the oil-trapping mechanism. The geometry of a fault system was derived from parametric inversion of gravity data. The magnetic anomalies were extended with the trends of NS, NW, and NE and reached a maximum value of 55 nT. However, the gravity anomalies appeared with the same extensions and values ranging from -3.3 to 1.5 mGal. The intense magnetic susceptibility amount of the reservoir rocks is arising from chemical processes and iron-oxide ion replacements, accompanied by the migration and accumulation of hydrocarbon. Incorporating the results from the Euler's depth estimation, parametric data modeling along with logging data assisted simultaneous modeling of the magnetic and gravity data. The 2D geological model of the subsurface layers at the Kifl area presents a graben-horst fault system within a thick sequence of sediment. Geological characteristics extracted from geophysical data modeling provided insightful information on the nature and essence of the hydrocarbon reservoirs in the Kifl area. It has formed through tectonic deformation and tension over the Arabian plate during the Permian – Paleocene cycle. Hence, it can be concluded that the aforementioned fault system has divided the hydrocarbon reservoirs.

Keywords: *Magnetic, Gravity, Inversion, Kifl area, Oil trapping.*

1. Introduction

The magnetic and gravity explorations are widely applied in many fields such as engineering purposes, exploration of minerals, ore-bearing bodies, hydrocarbon accumulation, groundwater, and delineating faults' locations and subsurface geological structures [1,2]. As an illustration, oil and gas reservoirs can be explored by the potential field exploration methods. Moreover, these geophysical techniques are advantageous methods to attribute the subsurface tectonic characteristic [3,4]. In oil surveys, these ways can be used to recognize the connection between complex fault configurations (e.g., [5,6]). Ali et al. (2014) used different types of filters and transformation techniques of gravity data, like the ones used in our research, to distinguish gravity anomalies in the UAE and identify source boundaries, as a tool to study the general structure of the region [7]. It should be noted that all these results were used in geological modeling. During the past years, the use of magnetic and gravity surveys has increased enormously, particularly in hydrocarbon exploration (e.g., [8-13]). There has been a continual interplay between developing geophysical instruments on the one hand and devising techniques to interpret the data on the other hand [14].

Interpretation of the magnetic and gravity data is essentially aimed to estimate the location and the depth of the causative sources [1], where retrieving the geometry of those sources is the ultimate motive. In

general, it appears that both magnetic and gravity methods are characterized by various kinds of interpretation techniques. Some of which are directly giving results but others require additional processes to reach the desired results. In practice, when conducting a magnetic or gravity survey, we will encounter several problems which might end in a great variety of interpretations. Consequently, method or methods should be executed which are closer to the reality of the studied target. As a result, reaching such a goal requires proper skill and craftsmanship in geophysics, as well as correct employment of geological information [15].

The main objective of this research is to model the magnetic and gravity data surveyed over the Kifl area in central Iraq to gain a better understanding of the main tectonic features which provides valuable insights into the location of probable reservoirs containing hydrocarbon accumulation. Determining the type of geological structures for the reservoirs is also of interest. Therefore, the magnetic and gravity surveys are employed to recognize the subsurface geological structures. Hence, different types of filters and analyses were used to reach geologically reasonable models. Filtering of the magnetic and gravity data is a base operation before data analysis and interpretation. The Euler deconvolution filters and INVGRAFALT program (as a Fortran-based

* Corresponding author: *E-mail address:* boskooi@ut.ac.ir (B. Oskooi).

code) were first used to estimate the depth of the sought geological structure along with the geometry of a causative fault in association with this structure. Finally, by incorporating the obtained results into the final modeling, the IGMAS+ software was used to model the potential field data simultaneously, where a cross-sectional model of the subsurface layers was deduced [16].

In the following sections of this research, numerical techniques were summarized in section two. Section three explains the geological descriptions of the Kifl oil field in Iraq. Potential field geophysical surveys are introduced in the fourth section, while Euler's depth estimation and parametric inversion of a causative fault structure are executed. Finally, in the last section, the geometry and tectonic setting of a hydrocarbon reservoir were imaged.

2. Methodology

2.1. Euler depth estimation

One of the substantial interpretation techniques is the Euler deconvolution of the magnetic and gravity data, using the directional derivatives of the observed data in order to estimate the depth to the top of causative sources responsible for potential field anomalies [2]. Thompson (1982) developed an approach to this method and utilized it along with line data [17]. Reid et al. (1990) pursued proposals in the work by Thomson and expanded the range to include the grids of potential field data. The Euler's equation homogeneity written in the following form can be implemented on the grid of the potential field data as [18]:

$$(x - x_0) \frac{\partial P}{\partial x} + (y - y_0) \frac{\partial P}{\partial y} + (z - z_0) \frac{\partial P}{\partial z} + nP = 0 \tag{1}$$

P is the potential field data, n indicates the amount of the predefined structural index (SI), (x_0, y_0, z_0) is the position of the source, and (x, y, z) is the coordinate of the field measurement. Here, Eq.1 gives a linear relationship between the SI and the unknown potential field, where the definition of SI is very important for solving this equation. Bearing in mind that it depends on the geometry of the underground source [18,19]. Here, the SI varies between 0 and 1 for gravity and magnetic anomalies, respectively. According to Thompson (1982) [17] listed in Table 1, different values of the SI are presented for various geometrical forms. Another important factor in optimizing the Euler solution is the correct choice for the used window size, discussed in detail by Bournas et al. (2003), [20].

2.2. Parametric data inversion

Chakravarthi and Sundararajan (2005) introduced "INVGRAFALT" code [21] based on Marquardt inversion (1963) [22], which has been used to determine four shape parameters including top, bottom, distance to the origin of the fault plane, and fault angle (Z_1, Z_2, D and i , respectively) of a faulted structure from gravity data, using the principles of the least-squares [23]. Gravity anomaly of a faulted bed (Figure 1) at any point $g(\hat{X}_k, 0)$ was given by Chakravarthi and Sundararajan (2004), wherein the density contrast varies parabolically with depth [23]:

$$g(\hat{X}_k) = \frac{2G\Delta\rho_0^2}{Q} \left\{ \frac{(S_1+S_2+S_3)}{S_6} \phi_2 + \frac{(S_1+S_4+S_5)}{S_7} \phi_1 + s \sin(i) \ln \frac{r_2 S_2}{r_1 S_6} \right\} + \sum_{n=0}^2 a_n \hat{X}_k^n \tag{2}$$

Table 1. Structural indexes for gravity and magnetic models [17].

No.	Geological geometry	Gravity	Magnetic
1	Horizontal contact with infinite dimensions	-1	0
2	Vertical contact	-1 - 0.5	0 - 0.5
3	Dyke - amorphous sill	0	1
4	Vertical cylinder	1	2
5	Amorphous cylinder	1.5	2.5
6	Horizontal cylinder	1 - 1.75	2 - 2.75
7	Point dipole - sphere	2	3

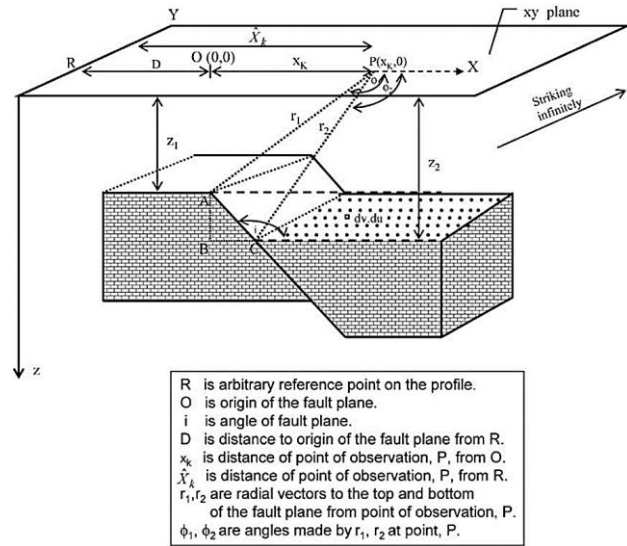


Figure 1. The geometry of a faulted bed (exactly inserted from [21]).

where $\sum_{n=0}^2 a_n \hat{X}_k^n$ is a polynomial for presenting regional background, and a_0, a_1 , and a_2 are coefficients of the polynomial. Also,

$$\begin{aligned} Q &= \Delta\rho_0^2 + 2s\Delta\rho_0 a \cos(i) + a^2 s^2 \\ s &= x_k \sin(i) - z_1 \cos(i) \\ s_1 &= \Delta\rho_0 s \cos(i) \\ s_2 &= a s (s + z_2 \cos(i)) \\ s_3 &= a z_2 \\ s_4 &= a s (s + z_1 \cos(i)) \\ s_5 &= a z_1 \\ s_6 &= \Delta\rho_0 - a z_2 \\ s_7 &= \Delta\rho_0 - a z_1 \\ r_1 &= (x_k + z_1^2)^{1/2} \\ r_2 &= (x_k + (z_2 - z_1) \cot(i)^2 + z_2^2)^{1/2} \\ \phi_1 &= \pi/2 + \tan^{-1}(x_k/z_1) \\ \phi_2 &= \pi/2 + \tan^{-1}(x_k + (z_2 - z_1) \cot(i))/z_2 \end{aligned}$$

This code has been used on synthetic and real gravity data whose results were geologically an acceptable model. The formulation of normal equations is as follows:

$$\sum_{k=1}^{N_{obs}} \sum_{j=1}^7 \frac{\partial g(\hat{X}_k)}{\partial a_j} \frac{\partial g(\hat{X}_k)}{\partial a_j} (1 + \delta_{jj} \lambda) da_j = \sum_{k=1}^{N_{obs}} [g_{obs}(\hat{X}_k) - g_{mod}(\hat{X}_k)] \frac{\partial g(\hat{X}_k)}{\partial a_j}, \quad j' = 1, \dots, 7 \tag{3}$$

Here, da_j ($j = 1, \dots, 4$) are increments to parameters Z_1, Z_2, D and i In addition, da_j ($j = 5, \dots, 7$) are increments to the coefficients of regional background, which are solved and subsequently added to existing parameters. Then, inversion repeats until the specified number of iterations is completed or the amount of misfit function falls below a predefined allowable error, or the damping factor attains a larger value.

Theoretical and observed gravity anomalies are $g_{mod}(\hat{X}_k)$ and $g_{obs}(\hat{X}_k)$, respectively. λ is the damping factor and its value is set to an arbitrary amount of 0.5. Note that (\hat{X}_k) is the distance of an observation point P from R (Figure 1). For more details about this equation see e.g. [21,23].

Gravity anomaly along a faulted bed can be simplified via the matrix notation as the following form,

$$g^{obs} = F(a) \tag{4}$$

Here, F is the forward operator matrix that maps from the model space into the data space g^{obs} . $a = [a_1, a_2, a_3, a_4]^T$ denotes the vector of known model parameters (Z_1, Z_2, D , and i). To estimate the unknown model parameters for observed gravity data along with a profile g^{obs} , the nonlinear relation can be replaced by a less ill-conditioned cost function to stably estimate parameters by minimizing the following equation,

$$\varphi(\mathbf{m}) = \varphi_d + \lambda\varphi_m, \quad (5)$$

where the misfit functional φ_d is defined as:

$$\varphi_d = \|(\mathbf{g}^{obs} - \mathbf{F}(\mathbf{a}))\|_2^2 \quad (6)$$

where λ as a damping factor should lead to a compromise between the data misfit norm and the model stabilizer norm (φ_m), [24]. A simple stabilizer norm can have the following formulation,

$$\varphi_m = \|(\mathbf{a} - \mathbf{a}_0)\|_2^2 \quad (7)$$

where \mathbf{a}_0 can be the initial model parameters. Equation 5 can be solved iteratively to update model parameters as,

$$\mathbf{a}^k = \mathbf{a}^{k-1} + \delta\mathbf{a} \quad (8)$$

Chakravarthi and Sundararajan (2004, 2005) implemented a Marquardt inversion approach to estimate the model parameters of a faulted bed [21,23].

2.3. Interactive data modeling

The IGMAS+ program is an indirect modeling method using experiment and error forward modeling, performed by the implementation of a numerical simulation of subsurface structures that are described as closed polyhedrons of constant susceptibility and/or density [25,26]. Alvers et al. (2010) [27] presented the new IGMAS+ (Interactive Geophysical Modeling Application System) system as a gravity/magnetic modeling program. Exemplary field data-set on which gravity/magnetic modeling has been successfully applied, are in sub-salt (e.g., [28,29]) and sub-basalt studies (e.g., [30]) for cases where seismic modeling suffers from the low resolution of subsurface layers. Ghazala et al. (2018) used the program to investigate the surface and subsurface structures in Sohag area, Egypt [31]. The extracted results showed the distribution of the fault segments and lines. Moreover, they gave a clear perception of the unequal style of the basement rock with different depths reflecting uplifted basement and down-faulted basins (horsts/grabens).

3. Geological setting of the Kifl oil field

The studied region is located in the center of Iraq (Figure 2), situated at the west of the Euphrates river, which is about 30 km far from the southwest of the Hilla city between Karbala and Najaf. The borders of the prospect region are limited by the latitude of 32° 08' 08" - 32°17' 03" N and the longitude of 44° 07' 50" - 44° 21' 07" E. Taking geology and tectonic settings of the Kifl area into account, sediments occur superficially from Eocene in the southwest to recent deposits on the Euphrates zone in the east. They often indicate a very slight dip towards the east and northeast (two degrees). Most of the faulted area has been covered by Quaternary sediments [32,33]. Figure 3 shows a simplified stratigraphic column of the Kifl area and adjacent areas, reported by Mobil Oil Company (1985) [34]. The faults belong to the Euphrates boundary as one of the most prominent Najd fault zones, which run toward the Euphrates River in the south of Iraq and continue towards the Rutba area in the west [35]. However, in adjacent areas, 49 normal faults have occurred with a general trend of NW-SE and N-S. These faults can be described as minor faults as well [36]. The investigated area is usually considered tectonically stable; additionally, the sedimentary cover ranges from 7-8 km overlying basement rocks [11].

The Kifl area is laying on the stable shelf within the Mesopotamian zone and in the Euphrates subzone. According to Jassim and Goff's division [35], it represents the boundary between stable and unstable shelf. The geological and tectonic evolution of Iraq is considerably influenced by the opening and closing of Palaeotethys and Neotethys oceans. The Neotethys was opened during the upper Carboniferous-Permian period along the rifting axis running parallel to Zagros, and when the Arabian plate was dominated by post-rift thermal sag. It led to generating a passive margin to the northwest and northeast, which progressively prograded basin wards from W/SW to the E/NE (Figure 4). The new Tethys ocean continued to spread to the NE, and the Mediterranean in the north began to open in the Late Jurassic. The Mesopotamian intercontinental basin developed inside the Arabian plate and at the west of the Zagros thrust zone. Consequently, the Kifl

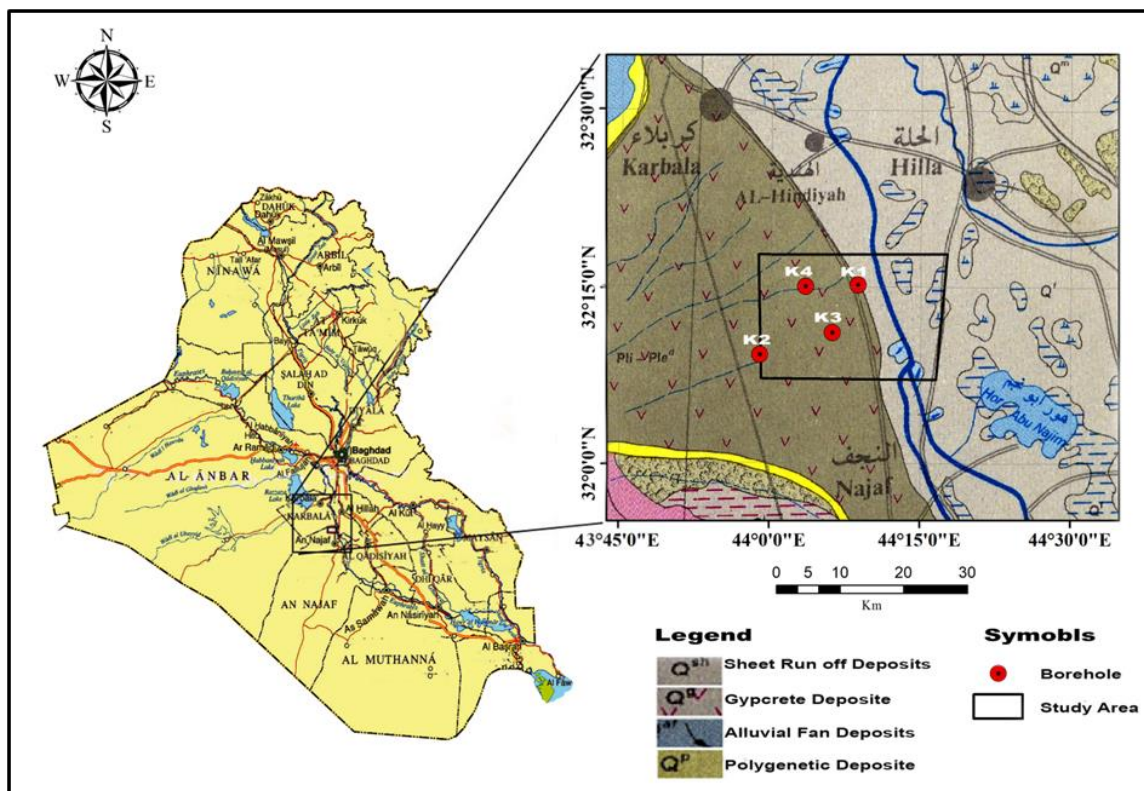


Figure 2. Simplified geological map of Iraq and the studied oil field in the Kifl region.

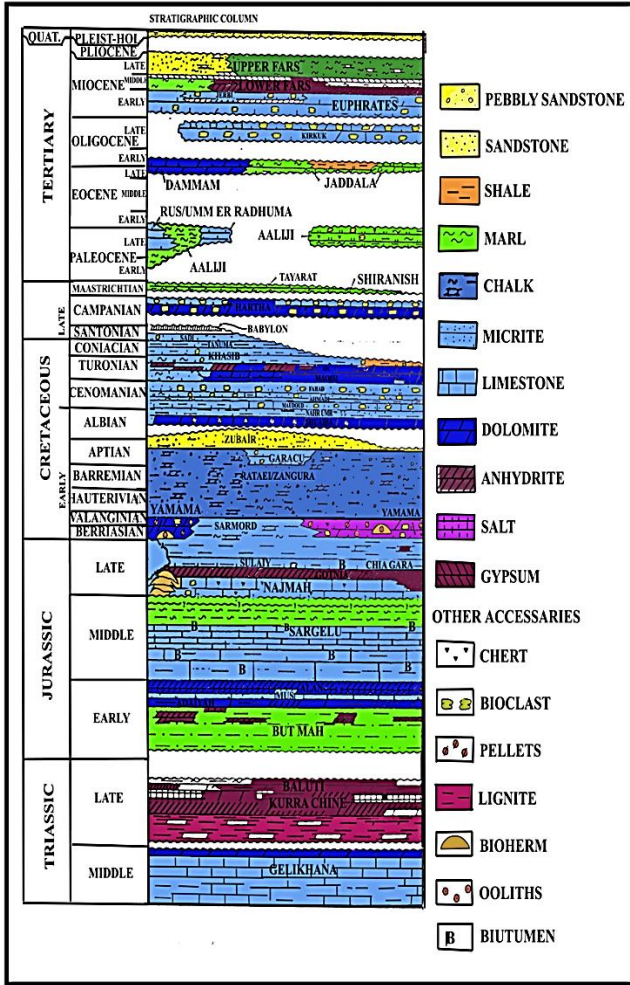


Figure 3. Stratigraphic column in the Kifl area (reported by [34]).

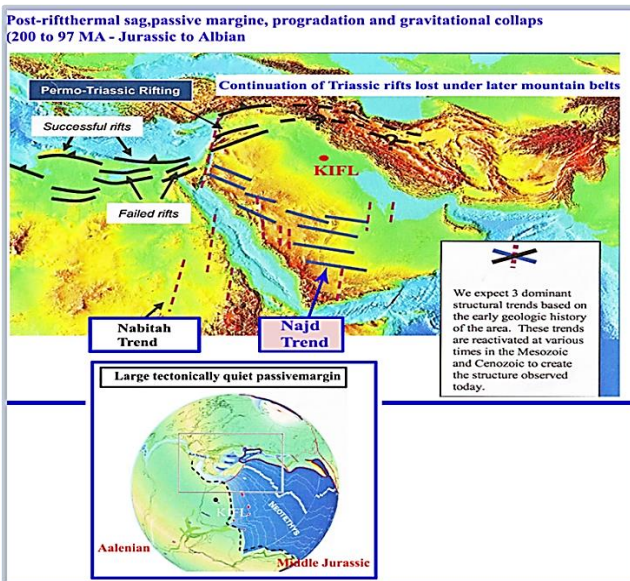


Figure 4. Post thermal sag (Sargelue – Nahr Umar [51]).

The transversal faults have played important roles in the depositional basin environment, and later in the development of the main tectonic structures. It means that the faults have been active since Permian [37].

area was affected by those movements. It was located on the west flank of the Mesopotamian basin.

The transversal faults have played important roles in the depositional basin environment, and later in the development of the main tectonic structures. It means that the faults have been active since Permian [37]. The main structural elements recognized and described up to now were mostly those caused, or at least to a different degree directly affected by the Alpine Orogenic phases, mainly by the tertiary ones. Therefore, the trends of the subsurface features in this block are parallel to the Alpine chain, prevalently NW-SE and N-S. The geological background of the area was affected by the geometry of the underground basement masses and faults. Moreover, it is also affected by the Palaeozoic epirogenic events and Mesozoic arching [35]. In the other word, the depositional setting and structural style of the study area has been influenced by four major tectonic movements summarized as follows;

1- Post rift thermal sag, passive margin progradation gravitational collapse (Lower Jurassic-Albian 97-200 million years), almost Sargelu-Nahr Umr formation (Figure4).

2- Opening on the south Atlantic drives subduction of NE Arabia plate, ophiolite obduction, and Arc collision (Cenmanian to middle Turonian 84-94 million years), almost Mudud-Tanuma Unconformity.

3- Rifting creating the Euphrates graben as collision wanes (Late Turonian to Maastrichtian 66-90 million year), almost Tanuma shale/sadi-Shiranish formation.

4- Multiple Cenozoic events: Syrian Arc contraction, Red Sea opening, Zagros collision and later strike-slip movements and Anatolian extrusion (Late Paleocene/Eocene to Pliocene/Recent 52 million years), almost Aaliji- surface formation.

In 1959, the K1 exploration well was drilled on the crest of this structure, which penetrates the mid-Jurassic-Triassic formations. The drilling reaches 3256.5 m at Sargelue formation, approving oil-trapping in Nahr Umar and Zubair formations. The estimated production is approximately 5600 b/d. Then, K2 well was drilled 13.5 km southwest of K1, without indicating oil-trapping since it lay outside the structure enclosure of the field. Both K1 and K2 were localized through interpretation of gravity and seismic surveys executed by IPC company in the late 1950s. Upon results of a seismic survey (1975), the K3 well was drilled to explore the Triassic reservoir and to evaluate the number of hydrocarbon accumulations that appeared at K1 well. The drilling reached 4330 m depth at Kura chine formation. According to the log interpretations, the oil indicator was 1.5m higher in the Zubair formation. In 1980 and 1982, the Mobil Company studied the area and attributed the presence of oil in the Zubair formation due to stratigraphic traps. Therefore, the K4 well was drilled. It lies 4 km west of K1 to ensure obtaining the longest oil column within the sand body. However, the results proved that the Zubair formation is structurally thick about 10 m in K4 relative to K1, while the oil column in K4 was 3 m. Note that the K4 well was drilled for the estimation of hydrocarbon accumulation in the Zubair and the Yamama formations, and to see how the oil was trapped [38]. Table 2 illustrates the well-drill information in the studied area.

4. Potential field Geophysical survey

We measured about 1080 magnetic data along 20 parallel profiles with a length of 16 km and an NS strike (Figure 5a). Station spacing was around 250 meters. In some places, the inter-distance was more/less than 250 m due to natural and artificial obstacles. Further data measurements were performed between the main profiles. It is also worth mentioning that the field staff benefited from the passable roads to accomplish the work field in less time, where the majority was towards the north-south. A proton magnetometer was used for a base station. This station was chosen in the middle of the studied area (Figure 5a). During the fieldwork, there was another group for measuring the data manually every ten minutes. The G858 Cesium portable magnetometer was used for this survey. The Earth's magnetic field intensity in the Kifl area is about 45,580 nT, while inclination and declination angles are 48.9° and 3.9°, respectively.

Table 2. Concise information of drilled wells in the Kifl Area (extracted from reports by Iraqi Geological Survey and Mine Research Company) [52].

Well	Longitude	Latitude	Year of drilling	Total depth (m)	Depth upper Zubair Fn. Below sea level (m)	Thickness Zubair Fn. (m)	Notes
Kifl 1	44°10' 55" E	32°14'59" N	1961	1515	1963	489	Product from the upper part of Zubair Fn.
Kifl 2	44°05' 37" E	32°09'36" N	1962	2715	1809	19	Non-product
Kifl 3	44°10' 00" E	32°12' 00" N	1980	3304	1961	442	Non-product
Kifl 4	44°07' 46" E	32°15'16" N	1984	4330	1924	466	Product from the upper part of Zubair Fn

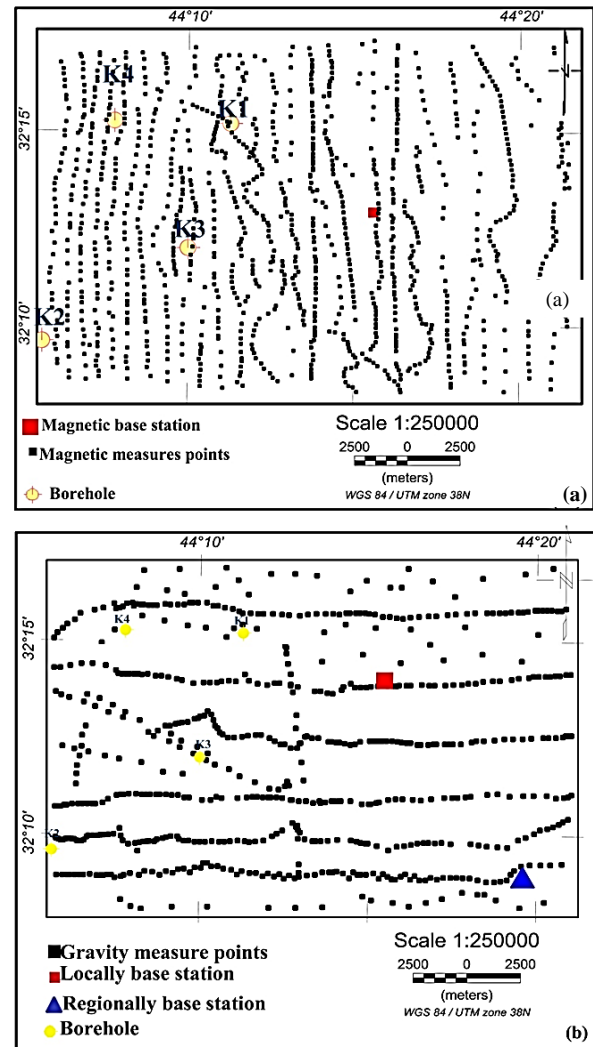
Gravity measurements were done for about 600 points along 6 profiles with a length of 24 km (Figure 5b). Figure 5b shows the distribution map of the gravity stations and the location of the local base station and regional base station. The direction of the profiles was EW with a station spacing of 250 m. The gravity profiles were oriented perpendicular to the magnetic profiles, and the main strikes of geological structures in the study area. A CG5 gravimeter was used for data measurement. The gravity survey started at the regional base station. This is for calibrating the instruments and relates the readings to the absolute gravity value. The State Company of Geological Survey and Mining gave us the location of the regional base station which is at 32° 08' 49" N and 44° 19' 10" E. The absolute gravity value at the regional base station (as given by GEOSURV) is 979467.910 mGals. The gravity readings at the local base station were measured every 1 to 2 hours. Although, the topography of the study area is characterized by semi-desert flat. A Surveying Engineer was hired to take an elevation of the area at five points (corners and center of the area). Furthermore, the elevation of the four Kifl wells, Najaf oil refinery, and the regional base station above sea level was used. The elevation was calibrated for all measuring stations by using the Garmin 76CSX GPS.

5. Magnetometry data interpretation

Collected data were processed for both magnetic and gravity surveys (Figures.6 and 7). The polynomial fitting method of the first order was used in the separation of the regional and residual data. It applies a digital filter on the observed data to subtract the long-wavelength anomalies associated with the regional field from the shorter wavelength anomalies associated with the target structure [39]. The total magnetic field intensity map and the residual magnetic anomalies have been presented in Figure 6a and b, respectively. In Figure 6b, sites 1 and 2 have symbolized a positive anomaly of about (55 nT), while location 3 displayed a minimum negative anomaly of about -60 nT. The most prominent anomalies in this map are several elongated and a few circular anomalies. At the first look at this map, a remarkable NS trend is observed, which is arising from two parallel faults, known as Hijaz fault system [37]. With another look at the magnetic map, these two NS trend anomalies are of limited extent. Along with the main features, many closed anomalies can be identified (apparent anticlines and synclines) which could represent local structures that are directly related to the movements of the fault. These suggested lineaments were parallel to the general structural trends that have been identified by Fouad (2010) in the nearby region (west of the study area) [33].

In Figure 6d, the analytic signal map (as the amplitude of directional derivatives) has been calculated for the reduced-to-pole (RTP) magnetometry data (Figure 6c), where the traces of structural lineaments have been superimposed on this map. Nabighian (1972 & 1974) proposed the concept of a 2D analytical signal filter for magnetic anomalies and later developed it for 3D cases investigated by potential field data [40,41].

The lineaments could be referred to as the NS faults in the study area. Another set of minor lineaments can be distinguished in the map, that is of NW and NE trends. According to Fouad's division (2010) [33], Mesopotamia basin faults are consisting of two main types trending, ENE-WSW, and NW-SE. The ENE-WSW trend fault has been explained by the presence of inverted folds and then has occurred fault-propagation. While another type of trend fault (NW-SE) has been described as forming grabens or half-grabens [42,43].

**Figure 5.** Locations of the magnetic (a) and gravity stations (b).

The Euler method was applied to estimate the depth of the potential anomalies resulting from magnetic and gravity data (Figures 8a and 8b, respectively). The number (0-1) was chosen for the SI that is equivalent to the decay rate of the potential field data by distance representing the existence of a contact surface, as stated by Thompson (1982) [17]. Such a selection was drawn based on the tectonic status of the studied area, as well as the interpretations and information extracted from the current study. As a final consequence, it can be claimed that the Kifl area is highly faulted, based on the above-mentioned analyses. Through this technique, it was found that most depths did not exceed 1000 m for these anomalies range. More details on the results out of the Euler method in our case indicate that the depth of the inner faulted zone is about 400-500 m, and has increased about 500-1000 m for the outer part. Note that we have only plotted depth estimates over the south oil target, which can help readers to not be confused.

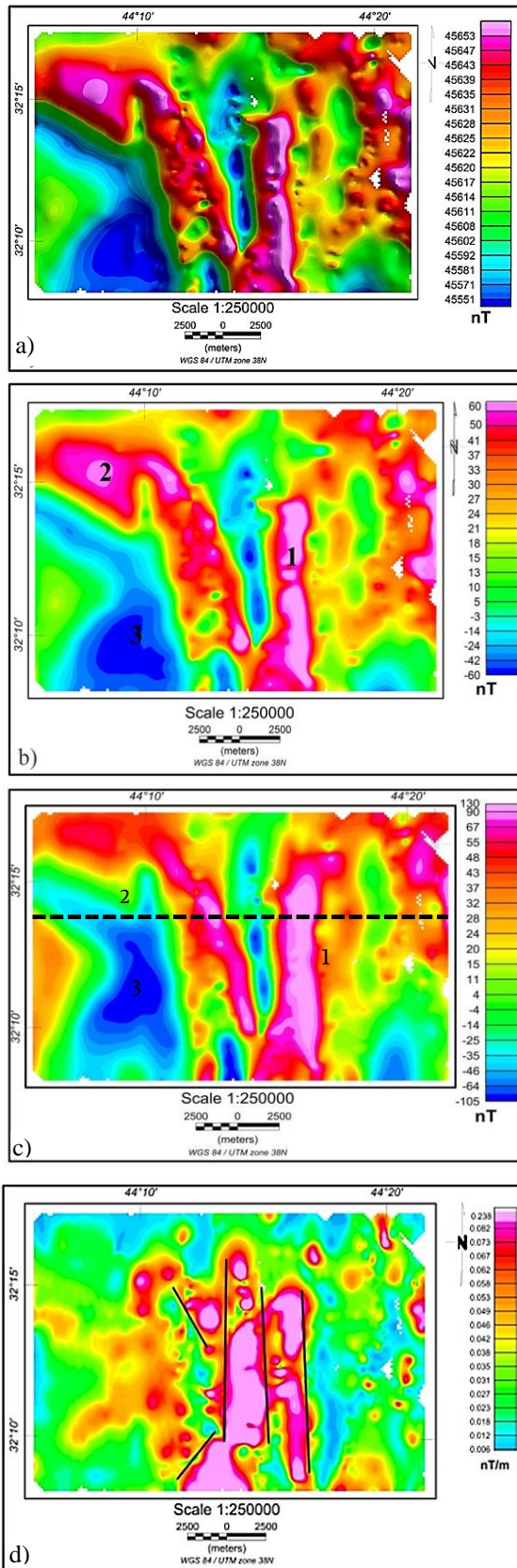


Figure 6. Magnetic data over the Kifl oil field, a) Total magnetic intensity map, b) Residual magnetic data, c) Reduced-to-pole magnetic data. The analytic signal map of the potential field data (d) has been shown for the reduced-to-pole filtering of the magnetic data on which the traces of the structural lineaments (solid line) have been superimposed. The dotted line in figure 6c is the modeling profile.

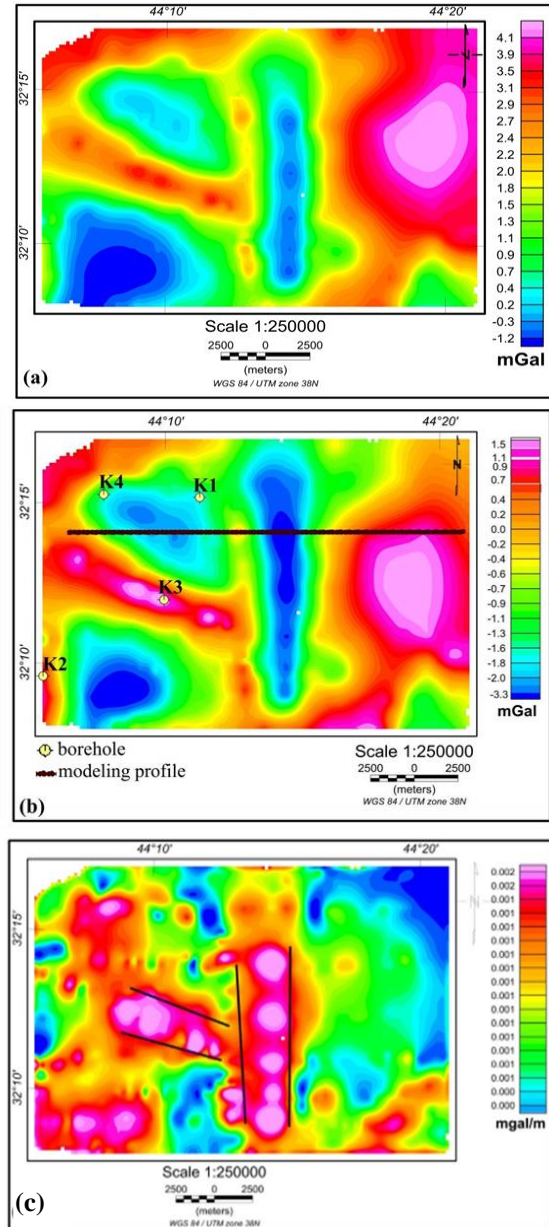


Figure 7. Gravity data over the Kifl oil field, a) Bouguer anomalies, b) Residual anomalies data and c) An analytic signal map. The traces of structural lineaments (solid lines) have been superimposed on the map. The dotted line in Figure 7b is the modeling profile.

5.1. Gravimetry data interpretation

In this work, in order to better understand the local structure, we have performed the residual-regional isolation. The residual anomalies map allows us to determine the most important local features of the Kifl area and obtain a suitable geometry of different underground structures. The act to separate the regional and the residual anomalies is an accurate side and important aspect of gravitational data explanation as much in-depth as on the surface, in a case to focus on the local subsurface structure [44]. Figure 7a and b show the Bouguer and residual anomaly maps, respectively. The main stage of gravity data processing is the residual anomaly preparation (Figure 7b), where the observations decline gradually towards the west, with values ranging from -3.3 to 1.5 mGal. The increasing trend is also from the west to east direction of the study area and the mean horizontal gradient in this direction is about 0.2 mGal/km. The increase in gravity values towards the east of the study

area was interpreted by Mousa et al. (2017) as an increase of the sedimentary column where basement depth becomes 8 km [11]. Tectonically speaking, as some researchers ([35,36]) have pointed out the existence of a deep fault going through the area, a fault with upthrown side to the east and a downthrown side to the west could explain this situation. Besides, the residual anomalies could be related to the shallow structures. Now, if the residual anomaly map is reviewed again, the presence of the anomalies in the middle of the map and northwest will be observed, which can be described as fault zones extending NS and NW, respectively. By a variety of local gravity anomalies, we note here that the study area is divided into three sections. The first one is located in the east which reflects a moderate positive contrast of density. It has been separated from the other anomalies at the west by a negative anomaly lying in the central part by the NS orientation previously discussed. The second part was represented by a positive anomaly having a higher value relatively, located in the second half of the center area and extending to the west. In the northwest area, there was another negative sign. In general, the residual anomaly map showed the same direction as the structures found in the magnetic anomaly map, by consideration of the difference in the anomalies over the west area.

As a magnetic method, we applied an analytical signal on the residual map, and we sketched the traces of structural lineaments. NS faults can be distinguished in this map (Figure 7c). It represents other faults of northwestern trends corresponding to the transversal, NW faults mentioned by other geoscientists ([35,37, 45]). Naturally, these features were formed from a collision between Arabian - Eurasian plates, taking the NW-SE trend [45].

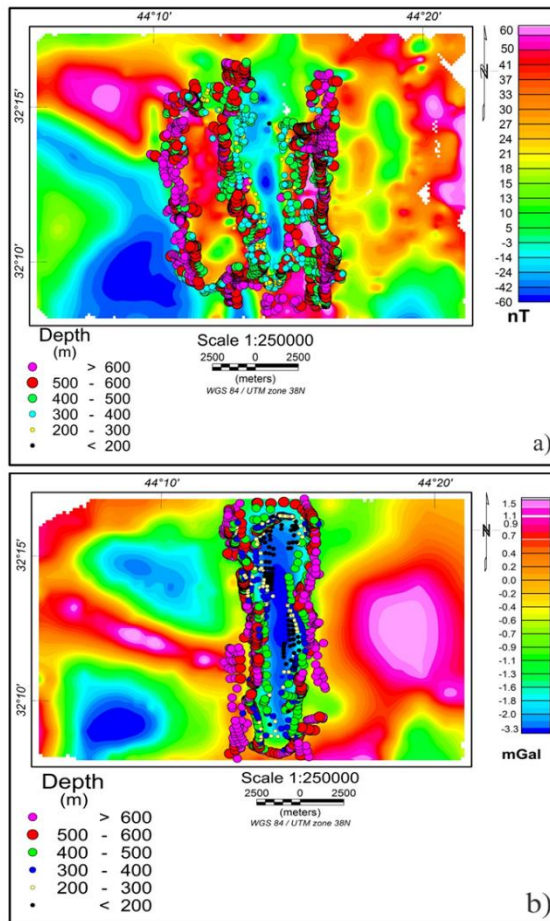


Figure 8. Euler depth estimation on the observed potential field anomalies, a) Magnetic data, and b) Gravity data. The window size is 10 and the SI range has been 0 and 1 for gravity and magnetic anomalies, respectively. Note that depth estimates were shown only for the sought oil-content target.

For confirming the previous results regarding gravity anomalies and estimating a fault parameter, a previously developed code "INVGRAFALT" based on the Marquardt inversion and presented by Chakravarthi and Sundararajan (2005), has been used to determine parameters (top, bottom, and fault angle) of a faulted zone [21]. Estimates substantially depend on the initially estimated depth of the anomalies from previous Euler results. We take this FORTRAN code, INVGRAFALT from the IAMG server, while the input and output parameters of the code were presented in Table 3. By applying this code, the results have been given somewhat a good match between observed and theoretical gravity anomaly values as shown in Table 3 and Figure 9, which plotted the real observations versus the calculated gravity values along with inferred fault model.

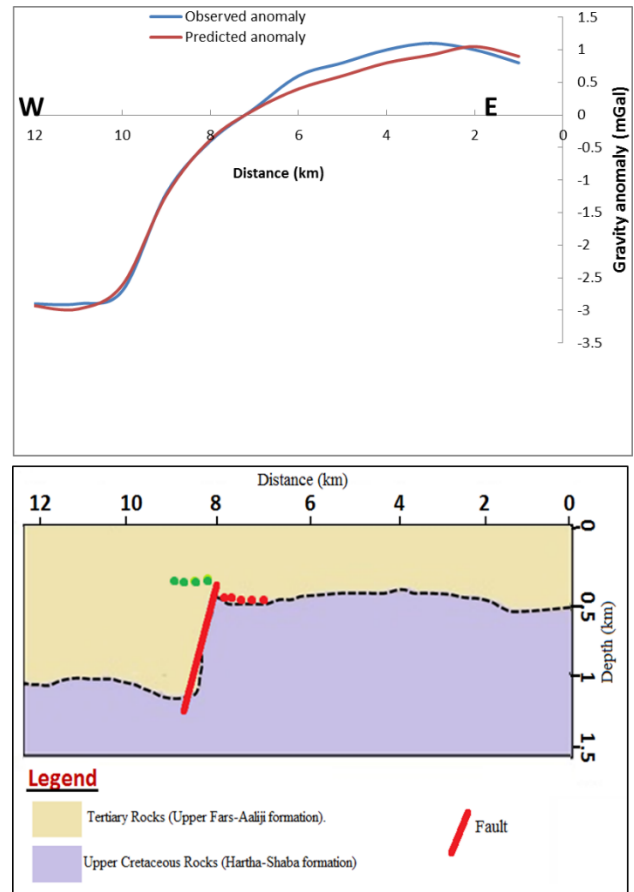


Figure 9. The curve of the observed and predicted gravity anomalies after parametric inversion of the faulted area with the inferred geological model along the half profile shown in Figure 7b from east to west of the area by assuming a density contrast 0.23 gm/cm^3 .

6. Discussion

The IGMAS+ software has been used here to model the causative source of the magnetic and gravity anomaly leading to the construction of the sub-surface layers of the studied area. This is done by employing all the results which are available from the interpretation of the previous methods and the geological information from well-drill in the Kifl area. Figure 10 depicts a model for a proposed cross-section of a long one profile in direction of EW of the investigated site where we take it from the RTP magnetic and residual gravity map (Figures 6c and 7b), respectively. As mentioned above, incorporating the available geological data from the well-drill in the Kifl area (especially the contrast values of density with depths) and the results of previous methods, which have described and estimated the shape and depth of the causative source in the area, interactive geophysical modeling was performed. All these data were applied to construct a model that simulates the oil trapping subsurface structure. We can summarize the type of data entered for model construction as follows:

Table 3. Assumed and estimated parameters for geophysical inverse modeling of faulted area.

Code's parameters				
No.	Input parameter	Initial value	Output parameter	Theoretical value
1	Number of observations	13	Number of observations	13
2	Distance to the observation point	13 km	Distance to the observation point	13 km
3	Approximate depth to top	0.4 km	Approximate depth to top in	0.403 km
4	Approximate depth to bottom	1.8 km	Approximate depth to bottom	1.019 km
5	Approximate fault angle	60°	Approximate fault angle	79°
6	Approximate distance to the center of the fault plane	10 km	Approximate distance to the origin of the fault plane	9.08 km
7	Surface density contrast in	-0.23 gm/cm ³		
8	Constant of parabolic density profile	0.15 gm/cc/ km		
Coefficients of the polynomial ($a_1=1.427$, $a_2=-0.263$, $a_3=0.001$)				
Observed anomaly			Theoretical anomaly	

- 1- Depending on contrast values of density, the site was divided into five layers (Table 4).
- 2- Magnetic susceptibility values were compiled from Hunt et al (1995) [46]. It is worth mentioning that the difference in formation lithology has an influential role in the susceptibility contrast. However, the susceptibility values were taken from standard divisions which is ranging from (0-50,000) *10⁻⁶ SI for sedimentary rocks.
- 3- Depth to top/bottom of suggested fault and angle was achieved from the results of the Euler deconvolution method and INVGRAFALT code.

Interpretation and analysis of any subsurface structures and sedimentary layer succession depend on the availability of information, whether geological, geophysical, or petrophysical properties of rocks. Therefore, we investigated the accuracy of applying these data to reach a well-fit and geologically reasonable model. Figures 10a and 10b show the magnetic and gravity data along with a profile that was taken from the residual gravity and magnetic maps in the EW direction of the study area with a length of about 22 km. This model was constructed based on the above-mentioned inputs as can be seen from this section (Figure 10c). The calculated and observed gravity/magnetic data have acceptable adaptation where we defined five layers for the geological model. However, in order to get the best fitness between the observed and calculated data, the depth of the subsurface layers has been altered. Furthermore, the main anomaly locates in the middle of the area in the form of a graben –horst structure. It has occurred through tectonic deformation and tension over the Arabian plate during the Permian – Paleocene cycle due to multiple Cenozoic events, namely Syrian Arc contraction, Red Sea opening, Zagros collision, and later strike-slip movements. Sedimentary speaking, considering the stratigraphy column of the area, we note that the depth and time of deposition of the Aliji formation have not exceeded the depth and occurrence time of the faults. We can say here, that deposition time for Aaliji formation is after faulting. The faults divide the hydrocarbon reservoirs.

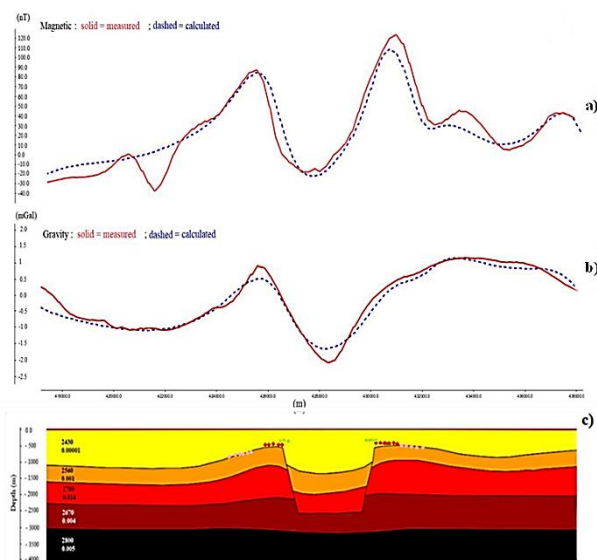
The top depth of the fault derived from the model is about 500 m which is closer to the Euler results. As shown in the graphs of the observed and calculated magnetic data, it is less matched than the gravity model. One of the reasons is the horizontal subsurface layers which lead to the decrease in the sensitivity of the gravity model. But depending on the changes in the susceptibility of each layer related to several lithologies in the observed magnetic model, and taking the average susceptibility for each layer of the calculated model, the mismatch between the observed and calculated magnetic data are more than those of gravity.

The magnetic susceptibility of rocks is controlled by the type and amount of magnetic minerals, where it reaches zero for sedimentary rocks. Faulting in the sediments is usually coincidental with the occurrence of high fracture intensity, corresponding to underground fluid passages and accumulations [47]. Here, the magnetic susceptibility of the third layer is higher than the rest, which is related to the underground fluid trapped. In other words, the increase in magnetic susceptibility values depends on the chemical processes accompanying

the migration of oil and iron oxide water within the source and carbon [48-50]. Note that we can rarely find out an oil reservoir in the world with such characteristics in generating a distinct magnetic anomaly.

Table 4. Geophysical characteristics of subsurface geological layers are shown in Figure 7.

	Depth (km)	Density (kg/m ³)	Geological time
1	0-0.6	2430	Quaternary- Tertiary
2	0.6-1	2580	Late Cretaceous
3	1-1.950	2780	Late Cretaceous- upper early Cretaceous
4	1.950-2.950	2670	Upper early Cretaceous- late Jurassic
5	2.950-4.000	2800	Late Jurassic-upper late Triassic

**Figure 10.** 2D cross-section views of the geological subsurface layers in the Kifl oil field c), and observed and predicted magnetic and gravity data along the desired profile in a) and b), respectively.

7. Conclusion

The ground-based magnetic and gravity survey for the western Kifl area indicated anomalies ranging from -60 to 55 nT for magnetic and -3.3 to 1.5 mGal for gravity data. The analytic signals of the potential field data presented three lineaments set with NS, NW, and NE trends. These features are attributed to be existed due to a result of a regional tectonic movement, so-called the collision of Iranian-Arabian plates, which in turn constructed the movement of the Hijaz mountain range. Euler

deconvolution for depth estimation of the major anomalies suggests a maximum of 1000 m. It means that the most anomalies in association with oil trapping have been placed within the sediments. We applied a code, INVGRAFALT, to gravity data to determine top, bottom, and fault angles where results were 403 m, 1,019 m, and 79°, respectively. The major potential anomaly was interpreted as related to the fault which is located in the sedimentary cover and has an extension toward the north-south of the study area. The IGMAS+ modeling was used to identify the shape and depth of this fault and sedimentary layer succession. Geophysical modeling results indicated a graben-horst oil-content reservoir where it cut the Tertiary rocks (Aaliji formation) and may be extended to 2500 m depth at the Cretaceous rocks (Yamama formation). In summary, it can be said that the results of IGMAS are more acceptable and closer to the geological reality in the oil field region.

Acknowledgment

We thank the Institute of geophysics, University of Tehran, and Babylon University for all their support, and Sabine Schmidt for permission to use the 3D gravity modeling program (IGMAS). The Department of the Ministry of Oil/Iraq for allowing us to read the reports and data is also appreciated.

REFERENCES

- [1] Nabighian M.N, Ander M. E, Grauch V. J. S, Hansen R. O, LaFehr T. R, Li Y, Pearson W.C, Peirce J. W, Phillips J. D, Ruder M. E (2005) Historical development of gravity method in exploration. *Geophysics* 70:63–89.
- [2] Wang J, Meng X, Li F (2017) New improvements for lineaments study of gravity data with improved Euler inversion and phase congruency of the field data. *Journal of Applied Geophysics* 136:326–334.
- [3] Finn C.A, Morgan L.A (2002) High-resolution aeromagnetic mapping of volcanic terrain, Yellowstone National Park: *Journal of Volcanology and Geothermal Research* 115: 207–231.
- [4] Ross G.M, Broome J, Miles W (1994) Potential fields and basement structure: Western Canada Sedimentary Basin: in Mossop, G.D., and Shetsen I, Compilers, *Geological Atlas of the Western Canada Sedimentary Basin*: Canadian Society of Petroleum Geologists and Alberta Research Council, 41– 46.
- [5] Spaid-Reitz M, Eick P.M (1998) HRAM as a tool for petroleum system analysis and trend exploration: a case study of the Mississippi Delta survey, southeast Louisiana. *Canadian Journal of Exploration Geophysics* 34:83–96.
- [6] Peirce J.W, Goussev A.A, McLean R, Marshall M (1999) Aeromagnetic interpretation of the Dianango Trough HRAM survey, onshore Gabon: *SEG Extended Abstracts* 18:343– 346.
- [7] Ali M. Y, Watts B, Farid A (2014) Gravity anomalies of the United Arab Emirates: Implications for basement structures and infra-Cambrian salt distribution. *Geo. Arabia* 19(1):85–112.
- [8] Stadler C, Fichler C, Hokstad K, Myrland E.A, Wienecke S, Fotland B (2014). Improved salt imaging in a basin context by high resolution potential field data: Nordkapp Basin, Barents Sea. *Geophys. Prospect.* 62: 615–630.
- [9] Hackney R, Goodwin J, Hall L, Higgins K, Holzrichter N, Johnston S, Morse M, Nayak G.K, Petkovic P (2015) Potential-field data in integrated frontier basin geophysics: Successes and challenges on Australia's continental margin. *Mar. Pet. Geol.* 59: 611–637.
- [10] Kovac P, Cevallos C, Feijth J (2016) Targeting oil and gas in the Perth Basin using an airborne gravity gradiometer. *First Break* 34: 51-58.
- [11] Mousa A, Mickus K, Al-Rahim A (2017) The thickness of cover sequences in the Western Desert of Iraq from a power spectrum analysis of gravity and magnetic data. *Journal of Asian Earth Sciences* 138:230–245.
- [12] Peng G, Liu Z, Xu K, Bai Y, Du R (2018) Efficient 3D inversion of potential field data using fast proximal objective function optimization algorithm. *J. Appl. Geophys.* 159: 108-115.
- [13] Ocaño F.M.O, Gallardo L.A, Romo-Jones J.M, Perez-Flores M.A (2019) Structure of the Cerro Prieto Pull-apart basin from joint inversion of gravity, magnetic and magnetotelluric data. *J. Appl. Geophys.* (in press).
- [14] Dobrin M.B, Savit C.H (1988) *Introduction to Geophysical Prospecting*. Fourth Edition. McGraw Hill Book Company, pp.865.
- [15] Gallardo L. A, Antonio M, Enrique T (2003) A versatile algorithm for joint 3D inversion of gravity and magnetic data. *Geophysical J.* 68:949–959.
- [16] Schmidt S, Götze H. J, Plonka C, Lahmeyer B (2011) Hybrid modelling of gravity, gravity gradients and magnetic fields. *Geophysical Prospecting* 59:1046–1051.
- [17] Thompson D.T (1982) EULDPH: A new technique for making computer-assisted depth estimates from magnetic data. *Geophysics* 47:31–37.
- [18] Reid A.B, Allsop J.M, Granser H, Millet A.J, Somerton I.W (1990) Magnetic interpretation in three dimensions using Euler deconvolution. *Geophysics* 55:80–91.
- [19] Oskooi B, Mirzaei M, Moghaddam M.M, Mohammadi B, Ghadim F (2015) Integrated interpretation of the magnetotelluric and magnetic data from Mahallat geothermal field, Iran. Article in *Studia Geophysica at Geodaetica*. DOI: 10.1007/s11200-014-1235-1.
- [20] Bournas N, Galdeano A, Hamoudi M, Baker H (2003) Interpretation of the aeromagnetic map of Eastern Hoggar (Algeria) using the Euler deconvolution, analytic signal, and local wavenumber methods. *J. Afr. Earth Sci.* 37:191–205.
- [21] Chakravarthi V, Sundararajan N (2005) INVGRAFALT–A Fortran code for Marquardt inversion of gravity anomalies of faulted beds with varying density. *Computers & Geoscience* 31:1234–1240.
- [22] Marquardt D.W (1963) An algorithm for least-squares estimation of nonlinear parameters, *J. Soc. Indian Appl. Math.* 11:431–441.
- [23] Chakravarthi V, Sundararajan N (2004) Ridge regression algorithm for gravity inversion of fault structures with variable density. *Geophysics* 69:1394–1404.
- [24] Oldenburg D.W, Li Y (2005) Inversion for applied geophysics: a tutorial. In: Butler, D. K. (Ed.), *Near-surface Geophysics*. SEG., pp. 89–150
- [25] Götze H.J, Lahmeyer B (1988) Application of three-dimensional interactive modelling in gravity and magnetics: *Geophysics* 53(8):1096–1108.
- [26] Schmidt S, Götze H. J (1998) Interactive visualization and modification of 3-D models using GIS functions. *Physics and Chemistry of the Earth* 23:289–295.
- [27] Alvers M.R, Schmidt S, Götze, H. J, Fichler C (2010) IGMAS+ software for 3D gravity, FTG and magnetic modeling–Towards semantic constraints. EGM 2010 International Workshop, Capri, Italy, Expanded Abstracts.

- [28] O'Brian J, Rodriguez A, Sixta D, Davies M. A, Houghton P (2005) Resolving the K-2 salt structure in the Gulf of Mexico. *The Leading Edge* 24:404–409.
- [29] Fichler C, Rueslatten, H, Gram C, Ingebrigtsen A, Olesen O (2007) Salt interpretation in the Nordkapp Basin, Barents Sea, with special focus on magnetic data. EGM International Workshop Innovation in EM, Gravity and Magnetic Methods: a New Perspective for Exploration, Capri, 16–18 April. Extended Abstract.
- [30] Marelllo L, Ebbing J, Gernigon L (2013) Basement inhomogeneities and crustal setting in the Barents Sea from a combined 3D gravity and magnetic model. *Geophys. J. Int.* 193: 557–584.
- [31] Ghazalaa H, Ismael M, Lameesa I, Haggaga M (2018) Structural study using 2D modeling of the potential field data and GIS technique in Sohag Governorate and its surroundings, Upper Egypt. *NRIAG Journal of Astronomy and Geophysics* 7:334–346.
- [32] Sissakian V. K, Mohammed B. S (2007) Geology of Iraqi Western Desert. *Iraqi Bull. Geol. Min. Special Issue*: 51–124.
- [33] Fouad S. F. A (2010) Tectonic and structural evolution of the Mesopotamia foredeep, Iraq. *Iraqi Bulletin of Geology and Mining* 6:41–53.
- [34] Mobil Oil Company (1985) Hydrocarbon Potential, West Baghdad Area, Central Iraq, O.E.C. documents, 32 p.
- [35] Jassim S.Z, Goff J. C (2006) Geology of Iraq, Czech Republic, ISBN 80-7028-287-8, pp 341. Prague, 35-52.
- [36] Al-Banna A (1992) Gravity lineaments, fault trends and depth of the basement rocks in Western Desert. *Iraqi J. Sci.* 33:63–79.
- [37] Hijab B. R, Aldabbas M. A (2000) Tectonic evolution of Iraq. *Iraqi Geological Journal* 32:26–47.
- [38] Oil Exploration Company (1991) Kifl 3D survey, pre- planning report, Geophysical study dept., O.E.C. document, 88p.
- [39] Li Y, Oldenburg D. W (1998) Separation of regional and residual magnetic field data. *Geophysics* 63(2):431–439.
- [40] Nabighian M.N (1972) The analytic signal of two-dimensional magnetic bodies with polygonal cross-section: Its properties and use for automated anomaly interpretation. *Geophysics* 37:507-517.
- [41] Nabighian M.N (1974) Additional comments on the analytic signal of two-dimensional magnetic bodies with polygonal cross-section. *Geophysics* 39:85-92.
- [42] Fouad S.F.A (2007) Tectonic and structural evolution, Geology of Iraqi Western Desert. *Iraqi Bull. Geol. and Min.* 1:29–50.
- [43] Fouad S.F.A, Nasir W.A.A (2009) Tectonic and structural evolution of Al-Jazira area. *Geology of Al-Jazira Area, Iraqi Bulletin of Geol. and Min.* 3:33–48.
- [44] Mallick K, Vasanthi A, Sharma K. K (2012) Bouguer Gravity Regional and Residual Separation Application to Geology and Environment. Capital Pub. Co. pp. 250.
- [45] Sissakian V, Al-Ansari N, Knutsson S (2014) Origin of Some Transversal Linear Features of NE-SW Trend in Iraq, and Their Geological Characters. *Natural Science* 6:996–1011.
- [46] Hunt Ch. P, Moskowitz B. M, Banerjee S. K (1995) Magnetic Properties of Rocks and Minerals. *Rock Physics and Phase Relations. A Handbook of Physical Constants. AGU Reference Shelf 3.* Copyright 1995 by the American Geophysical Union.
- [47] Al-Kubaisi M. S, Al-Jarah O. B, Abdul-Jabbar A. A (2014) Neotectonics of Al-Thirhar, Al-Habbaniya, Al-Razzazah Depressions, Central Iraq, by using Remote Sensing Data. *Iraqi Journal of Science* 55(2B):790–801.
- [48] Liu Q, Chan L, Li H, Wang F, Zhang S, Xia X, Cheng T (2004) Relationship between magnetic anomalies and hydrocarbon microseepage above the Jingbian gas field, Ordos basin, China. *AAPG Bulletin* 88:241–251.
- [49] Schneider J, Bechsta T, Machel H. G (2004) Covariance of C- and O-isotopes with magnetic susceptibilities a result of burial diagenesis of sandstones and carbonates: an example from the Lower Devonian La Vid Group, Cantabrian Zone, NW Spain. *Int. J. earth Sci.* 93:990–1007.
- [50] Schumacher D (1996) Hydrocarbon-induced alteration of soils and sediments in Hydrocarbon migration and its near surface expression. *AAPG Memoir* 66:71–89.
- [51] Sharland P. R, Archer R, Casey D. M, Hall S. H, Heward A. P, Horbury A. D, Simmons M.D (2001) Arabian Plate Sequence Stratigraphy. *GeoArabia Special Publication 2, Gulf Petrolink, Bahrain*, 371 p.
- [52] Iraqi Geological Survey and Mine Research Company (1990) Internal report of Kifl oil field. 38pp.